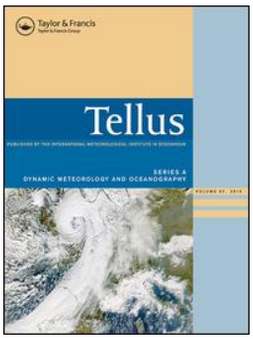

Tellus A: Dynamic Meteorology and Oceanography

ISSN: (Print) 1600-0870 (Online) Journal homepage: https://www.tandfonline.com/loi/zela20

On the parameterization of the radiative properties of broken clouds

Johannes Schmetz

To cite this article: Johannes Schmetz (1984) On the parameterization of the radiative properties of broken clouds, Tellus A: Dynamic Meteorology and Oceanography, 36:5, 417-432, DOI: 10.3402/tellusa.v36i5.11644

To link to this article: https://doi.org/10.3402/tellusa.v36i5.11644

Tellus (1984), *36A*, 417–432

On the parameterization of the radiative properties of broken clouds

By JOHANNES SCHMETZ, *Max-Planck-Institut für Meteorologie, Bundesstrasse 55, 2 Hamburg 13, F.R. Germany*

(Manuscript received November 15, 1983; in final form April 17, 1984)

ABSTRACT

A one-dimensional radiative transfer scheme is presented which accounts for the effects of broken cloud in the solar and infrared radiation field. The fractional cloud amount is explicitly considered in the two-stream model by treating clouds as the boundary condition between two adjacent atmospheric layers. The scheme accounts for absorption and scattering by gases and aerosols assuming realistic atmospheres. The radiative properties of broken clouds are included in a parameterized form making use of results from three-dimensional radiative transfer models. The radiative characteristics of a cloud field are represented by an average finite cloud whose size or optical thickness grows with increasing cloud amount. This growth is described by a simple mathematical model, and its use yields qualitative agreement between model results and observations for solar radiation.

The scheme is then applied to calculate the net radiative effect of broken cloud. Since the cloud size growth with cloud amount implies a non-linear relation between the fractional cloud amount and the radiative properties of the cloud field, the net radiative effect of cloud depends on cloud amount. The idealized model shows that the albedo effect (increase of solar reflection with cloud amount) of broken cloud is smaller than that of a plane-parallel cloud for cloud amounts less than about 0.7, while the opposite is true for larger cloud amounts. The greenhouse effect (reduction of the outgoing long-wave flux) of broken cloud is larger than that of a plane-parallel cloud for small cloud amount and smaller for large cloud amount.

An application of the radiation scheme to compute bispectral curves of visible albedo versus thermal brightness temperature shows that broken cloud layers and unbroken layers with variable optical depths show a similar shape of the bispectral curve.

1. Introduction

Since clouds are the most effective modulators of the atmospheric radiation field, accurate parameterizations for the computation of the radiative properties of clouds are required. One problem are the fields of finite clouds which often occur over wide regions of the globe. Theoretical studies of the solar (e.g., Busygin et al., 1973; McKee and Cox, 1974; Davies, 1978; Gube et al., 1981; Welch and Zdunkowski, 1981) and the infrared (e.g. Harshvardhan and Weinman, 1982a) radiative transfer through finite clouds have shown that the effect of cloud sides is to change the radiative properties significantly from what is observed for horizontally extended clouds. Since three-dimensional radiative transfer schemes are expensive, simple parameterizations for the use in one-dimensional schemes are desirable.

The present study outlines a detailed one-dimensional radiative transfer scheme which takes fractional cloud amount explicitly into account. The effect of fields of finite clouds can be accounted for in a one-dimensional scheme defining an effective cloud amount which is used instead of the actual cloud amount (that is the vertical parallel projection of the cloudy area). Such a parameterization for the solar radiation is derived from Monte Carlo calculations for finite clouds; for the thermal radiation, a parameterization after Harshvardhan and Weinman (1982a) is used.

We will not follow the commonly used concept

of a regular array of identical cuboidal clouds (e.g. Harshvardhan, 1982), but rather assume that the cloud field is represented by an average cloud which becomes larger as cloud amount increases (e.g., Plank, 1969). This results in a non-linear dependence of the solar effective cloud amount on the actual cloud amount, with the actual cloud amount always being larger than the effective cloud amount, which is contrary to previous parameterizations (Harshvardhan, 1982).

Similar to the work of Harshvardhan (1982), the influence of brokenness on the net radiative effect of cloud is studied. An extension is the use of the new parameterization of effective cloud amount within the frame of the detailed radiation scheme. This allows for interactions between cloud fields, surface and the atmosphere and makes a quantitative estimate of the change of radiation budget parameters possible. Furthermore, bispectral curves for the idealized cloud structures are computed and the possibility of deriving information on the spatial cloud structure from simultaneous visible and infrared satellite measurements are discussed.

Before we start describing the radiation scheme, some aspects of the cloud radiation problem in climate studies will be presented.

2. Radiation and clouds

Clouds have two different effects on the local radiation balance at the top of the atmosphere. First, the total solar absorption is reduced by clouds due to the increased reflection of solar energy. Second, clouds generally cause a decrease of the outgoing long-wave radiation due to their opacity with respect to terrestrial radiation. The first effect is known as the "albedo effect" of clouds and the second effect is called the "greenhouse effect". Since both effects act in different directions, the question arises concerning what net cloud effect occurs due to a change in cloudiness. The answer to this question is of importance, since it determines an eventual cloud-radiation feedback mechanism. This feedback mechanism could either dampen or enhance the climate sensitivity to changes in temperature due to variations of the solar constant, CO_2 increase or due to internal variations. Even a small local net effect of cloud on the earth's radiation budget could be very effective, since clouds cover about 50% of the earth.

There are different ways to get an estimate of the net effect of cloud. Wetherald and Manabe (1980) employed a general circulation model which predicts cloud height and cloud amount but used fixed optical cloud properties. Their results indicate that from equator to 50° latitude, a CO_2 increase reduces the net cloud amount and the effective cloud height because of a temperature increase. However, the increased long-wave loss to space is balanced by the increased solar absorption. Poleward of 50°, the net cloud amount increases, but again increased greenhouse effect and decreased solar absorption compensate each other. Thus, the cloud climatology changed, but the radiation budget of the earth did not. In that context one should note that a change in cloud climatology possibly implies a significant change in the local radiative forcing of the circulation without changing the earth's radiation balance.

Herman et al. (1980) have found a dominant albedo effect for a one-month wintertime simulation with a GCM. They have compared a control run including an interactive cloud-radiation scheme with two runs neglecting the solar and thermal radiative processes, respectively. Other model studies also suggest the importance of modeling the cloud-radiation feedback (e.g., Hunt, 1982; Wang et al., 1981; Fouquart and Morcrette, 1981; Geleyn et al., 1982).

Another approach to estimating the net change of the radiation balance due to a cloud change involves empirical studies using earth radiation budget data. Cess (1976) has suggested a solar-infrared compensation on a global average, while recently Hartmann and Short (1980) and Ohring and Clapp (1980) have found evidence for a dominant solar effect.

Schneider (1972) has introduced a cloud sensitivity parameter δ which determines the effect of a change in cloud amount N on the net radiation at the top of the atmosphere:

$$\delta = \frac{\partial(\text{net})}{\partial N} = \frac{\partial Q_{\text{abs}}}{\partial N} - \frac{\partial F}{\partial N}, \qquad (1)$$

where ∂(net) is the change in net radiation, N is the cloud amount, Q_{abs} is the solar absorption by the earth-atmosphere system and F the long-wave loss to space. Eq. (1) may be written as

$$\delta = -Q_0 \frac{\partial \alpha}{\partial N} - \frac{\partial F}{\partial N} = -\frac{\partial \alpha}{\partial N}\left(Q_0 + \frac{\partial F}{\partial \alpha}\right), \qquad (2)$$

where Q_0 is the solar flux at the top of the atmosphere and α the planetary albedo.

Q_0 can easily be calculated, and $\partial F/\partial\alpha$ can be derived from satellite data, although it might be difficult to get this partial derivative while holding other variables constant. Ohring and Clapp (1980) approached this partial derivative using individual monthly data from NOAA satellites and calculating the changes in F and α for the same month in successive years in selected geographical regions.

In order to arrive at an estimate for δ, some functional relation for $\partial\alpha/\partial N$ has to be assumed. Ohring and Clapp (1980) used the constant value:

$$\frac{\partial\alpha}{\partial N} = \alpha_c - \alpha_s, \tag{3}$$

where α_c is the planetary albedo for cloudy and α_s the planetary albedo for clear sky; both values are specified for different latitudes from climatological data.

In Section 8 of this paper, the radiation scheme is used to study the dependence of $\partial\alpha/\partial N$, $\partial F/\partial N$ and δ on cloud amount, that is to say the sensitivity of these parameters to broken cloud is studied.

3. The radiative transfer scheme

The transfer of diffuse radiation, neglecting azimuthal dependence, is described by the equation:

$$\mu\frac{dL(\tau,\mu)}{d\tau} = L(\tau,\mu) - \frac{\tilde{\omega}}{2}\int_{-1}^{1} p(\mu,\mu')\,L(\tau,\mu') \times d\mu' - J(\mu), \tag{4}$$

where L is the radiance, τ the optical depth, μ' and μ the cosines of the angles of the incident and the scattered radiation (positive for the upward radiation), $\tilde{\omega}$ is the single scattering albedo, $p(\mu,\mu')$ is the scattering phase-function and $J(\mu)$ the source function which for solar radiation is:

$$J(\mu) = \frac{\tilde{\omega}}{4\pi} S_0\,p(\mu,-\mu_0)\exp(-\tau/\mu_0), \tag{5}$$

and for terrestrial radiation:

$$J = (1-\tilde{\omega})\,B(T)/\pi. \tag{6}$$

S_0 is the solar intensity at $\tau = 0$, μ_0 the cosine of the solar zenith angle θ_0, and $S = \mu_0 S_0$ is the direct solar flux density. $B(T)$ is the black-body radiative flux and T the temperature. Integration of eq. (4) over both hemispheres, together with a quadrature solution to the integral describing the scattering of diffuse radiation yields the common coupled differential equations for the two-stream methods (e.g., Zdunkowski et al., 1980):

$$\frac{dM^+}{d\tau} = \frac{M^+}{\bar{\mu}}\{1-\tilde{\omega}(1-\beta)\} - \frac{M^-}{\bar{\mu}}\tilde{\omega}\beta - \gamma_1 Q, \tag{7}$$

$$\frac{dM^-}{d\tau} = \frac{M^+}{\bar{\mu}}\tilde{\omega}\beta - \frac{M^-}{\bar{\mu}}\{1-\tilde{\omega}(1-\beta)\} + \gamma_2 Q, \tag{8}$$

where M^+ and M^- are the upward and downward flux densities, respectively. For solar radiation, one finds:

$$\gamma_1 = \beta_0 = 1 - \gamma_2, \tag{9}$$

$$Q = \tilde{\omega}S_0\exp(-\tau/\mu_0), \tag{10}$$

and for terrestrial radiation:

$$\gamma_1 = \gamma_2 = 1.66(1-\tilde{\omega}), \tag{11}$$

$$Q = B(T,\tau) \simeq B(T,0) + \frac{\partial B}{\partial\tau}\Delta\tau. \tag{12}$$

$1/\bar{\mu}$ is chosen as 2 for the solar and 1.66 for terrestrial radiation. The back-scattering coefficients for the direct (β_0) and the diffuse radiation (β) are calculated from the phase function which is expanded in Legendre polynomials and truncated after the second term:

$$p(\mu,\mu') = 1 + 3g\mu\mu', \tag{13}$$

$$\beta_0 = \tfrac{1}{2}\int_0^1 p(\mu_0,-\mu')\,d\mu' = 0.5 - \tfrac{3}{4}g\mu_0, \tag{14}$$

$$\beta = \int_0^1 \beta_0\,d\mu = 0.5 - \tfrac{3}{8}g, \tag{15}$$

where g is the asymmetry parameter of the phase function.

In our calculations, the well-known delta-approximation to the phase function is used (e.g. Potter, 1970) which significantly improves the results in cases of the highly asymmetric phase-functions, and implies only a simple transformation of the model input parameters $\tilde{\omega}$, τ and g. The transformation of g avoids unphysical values of β_0 for $g \geqslant 0$ which is an appropriate range of g in atmospheric radiative transfer.

The solutions to eqs. (7) and (8) for the solar diffuse fluxes are:

$$M^+ = C_1 \exp(\varepsilon_1 \tau) + C_2 \exp(\varepsilon_2 \tau) + S\xi_1 \exp(\varepsilon_3 \tau),$$

$$M^- = C_1 \frac{a_2}{a_1 + \varepsilon_1} \exp(\varepsilon_1 \tau) + C_2 \frac{a_2}{a_1 + \varepsilon_2} \times \exp(\varepsilon_2 \tau) + S\xi_2 \exp(\varepsilon_3 \tau), \quad (16)$$

where ε_i are the eigenvalues of the differential equation system consisting of eqs. (7) and (8) and the differential equation for the direct solar flux:

$$\varepsilon = \varepsilon_1 = -\varepsilon_2 = (a_1^2 - a_2^2)^{1/2}, \quad (17)$$

$$a_1 = \frac{1}{\bar{\mu}} \{1 - \tilde{\omega}(1 - \beta)\}, \quad (18)$$

$$a_2 = \frac{1}{\bar{\mu}} \tilde{\omega}\beta, \quad (19)$$

$$\varepsilon_3 = -1/\mu_0, \quad (20)$$

$$\xi_1 = \frac{\mu_0(a_1 a_3 + a_2 a_3) - a_3}{\varepsilon^2 \mu_0^2 - 1}, \quad (21)$$

$$\xi_2 = \frac{\mu_0(a_1 a_4 + a_2 a_3) + a_4}{\varepsilon^2 \mu_0^2 - 1}, \quad (22)$$

$$a_3 = \tilde{\omega}\beta_0, \quad (23)$$

$$a_4 = \tilde{\omega}(1 - \beta_0) \quad (24)$$

For an inhomogeneous atmosphere, boundary conditions exist between two adjacent layers for the upward and downward diffuse fluxes:

$$M_i^+(\tau = \Delta\tau_i) = M_{i+1}^+(\tau = 0),$$

$$M_i^-(\tau = \Delta\tau_i) = M_{i+1}^-(\tau = 0), \quad (25)$$

where the layer index i is counted downwards. Eq. (25) and the boundary conditions at the top of the atmosphere and at the surface build up a linear equation system which is to be solved to get the coefficients C_i in eqs. (16).

The present solar and infrared schemes have already been compared with aircraft measurements and with other radiative transfer schemes (Slingo et al., 1982; Schmetz et al., 1981), and good agreement was obtained.

4. Parameterization of fractional cloud amount

Since the model is employed to study the sensitivity of the radiation field to cloud structure, it must account for fractional cloud amount.

Although the radiation schemes are one-dimensional, the horizontal cloud distribution can be explicitly taken into account if the clouds are considered with their bulk radiative properties (i.e., T = transmittance, R = reflectance, A = absorptance, E = emittance) as boundary conditions between two atmospheric layers (Schmetz and Raschke, 1979). For solar radiation, eqs. (25) are replaced by:

$$M_{i+1}^- = M_i^- T_1 N + M_i^-(1 - N) + M_{i+1}^+ R_1 N + S_i T_2 N,$$

$$M_i^+ = M_{i+1}^+ T_1 N + M_{i+1}^+(1 - N) + M_i^- R_1 N + S_i R_2 N, \quad (26)$$

where:
R_1 = reflection for diffuse radiation,
R_2 = reflection for direct radiation,
T_1 = diffuse transmission for diffuse radiation,
T_2 = diffuse transmission for direct radiation,
T_3 = direct transmission,
N = cloud amount.

For the direct solar flux S at a boundary containing clouds, the following holds:

$$S_{i+1} = S_i\{(1 - N) + T_3 N\} \quad (27)$$

Relations similar to eqs. (26) are obtained for the long-wave radiation.

The treatment of clouds as an infinitely thin layer between two model layers through eqs. (26) does not increase the computational effort which is needed to solve the linear equation system for the coefficients C_i, i.e., the computer run time is not increased. Eqs. (26) imply a random overlap in case of multi-layered clouds.

The optical properties of clouds are determined from a one-layer two-stream model, using the cloud's optical depth τ, the single scattering albedo $\tilde{\omega}$ and the asymmetry parameter g as model input, and again use is made of the delta-approximation to the phase-function.

R_1 and T_1 are computed from the boundary

condition that only diffuse radiation enters the cloud top; we then have:

$$R_1 = \{b_1 - b_2 \exp(2\varepsilon\tau)\}^{-1} + \{b_2 - b_1 \exp(-2\varepsilon\tau)\}^{-1}, \quad (28)$$

$$T_1 = \frac{(1 - b_2^2)\exp(\varepsilon\tau) + (1 - b_1^2)\exp(-\varepsilon\tau)}{2 - b_1^2 \exp(-2\varepsilon\tau) - b_2^2 \exp(2\varepsilon\tau)}. \quad (29)$$

where:

$b_1 = (a_1 - \varepsilon)/a_2$, $b_2 = (a_1 + \varepsilon)/a_2$.

The absorption A_1 is:

$$A_1 = 1 - R_1 - T_1. \quad (30)$$

The infrared emittance is analogously determined by:

$$E = 1 - R_1 - T_1. \quad (31)$$

The optical cloud properties for the direct solar flux are calculated from eqs. (16) using the boundary conditions $M^+(\tau) = 0$ and $M^-(0) = 0$, i.e., only a direct radiative component enters at the cloud top:

$$R_2 = \frac{p_1(\xi_1 p_4 - \xi_2 a_2) + p_2(\xi_2 a_2 - \xi_1 p_5) - 2\xi_1 \varepsilon T_3}{p_4 p_1 - p_5 p_2}, \quad (32)$$

$$T_2 = \frac{p_1(\xi_2 p_4 - \xi_1 a_2)\, T_3 + p_2(\xi_1 a_2 - \xi_2 p_5)\, T_3 - 2\xi_2 \varepsilon}{p_4 p_1 - p_5 p_2}, \quad (33)$$

$p_1 = \exp(\varepsilon\tau)$, $p_4 = a_1 + \varepsilon$,

$p_2 = \exp(-\varepsilon\tau)$, $p_5 = a_1 - \varepsilon$;

$T_3 = \exp(-\tau/\mu_0)$ is the direct transmittance.

The absorptance for the direct solar flux is then:

$$A_2 = 1 - T_2 - T_3 - R_2. \quad (34)$$

Eqs. (28)–(30) and (32)–(34) enable us to calculate the optical properties of clouds from the microphysical parameters for both the solar and infrared radiation. This consistent albedo-emittance relationship is a precondition for answering the question of the net radiative effect of clouds.

4.1. *Testing the parameterization of fractional cloud amount*

In Table 1, the parameterization of fractional cloud amount is compared with the results of the same model in resolving vertical cloud structure. The cloud has an optical depth of $\tau(0.55\ \mu m) = 30.5$, and $\tau = 2.7$, respectively, and the droplet size distribution corresponds to that measured within a stratocumulus top (Schmetz et al., 1981). The solar zenith is $\theta_0 = 51.1°$. The cloud is considered as a boundary condition at a height of 900 m, whereas the vertically-resolved cloud extends from 450 to 875 m. A standard mid-latitude summer profile is used, but no aerosol is considered. Table 1 reveals that the parameterization of cloud as infinitely thin layers gives good results for the upward fluxes, and thus also for the planetary radiation budget which is of most interest in this study. The error in the long-wave divergence and the solar convergence within the cloudy layer is larger since the radiative penetration depth is reduced for the parameterized cloud; however, the effects balance one another. The relative accuracy of the parameterization is slightly better for the optically thick cloud than it is for the thin cloud.

Table 1. *Comparison between radiative transfer calculations for different treatments of the cloud layer*
The solar zenith is 51.1° and a profile characteristic of a mid-latitude summer atmosphere is used.

	Planetary albedo (%)	Short-wave surface irradiance (W m^{-2})	Short-wave convergence between 0 and 1 km (W m^{-2})	Outgoing long-wave flux (W m^{-2})	Long-wave surface irradiance (W m^{-2})	Long-wave divergence between 0 and 1 km (W m^{-2})
$\tau = 30.5$						
Cloud vertically resolved	57.8	146	41	268	417	89
Cloud as boundary condition	58.3	144	37	267	413	85
$\tau = 2.7$						
Cloud vertically resolved	23.8	499	28	269	407	80
Cloud as boundary condition	24.4	481	24	268	404	75

5. Further model properties

The scheme has 37 spectral subintervals in the solar region (0.2–3.58 μm) and 50 subintervals in the thermal infrared (4–400 μm). For the results presented in the following sections, a C.1 droplet size distribution typical for low-level cumulus clouds (Deirmendjian, 1969) is used.

The model accounts for all important gaseous and aerosol extinction processes. The aerosol profile is a maritime standard atmospheric profile with a sea-level visibility of 23 km after McClatchey et al. (1980).

6. The Monte Carlo simulation

To study the radiative characteristics of three-dimensional clouds, a 3-d model is required. An appropriate approach is the Monte Carlo method (e.g., Marchuk et al., 1980), which treats the transfer of photons as a Markov process. Basically, photons are traced and scattering and absorption events are determined by the scattering phase-function and the single scattering albedo. The advantage of the Monte Carlo method is that it can easily be used to simulate the radiative characteristics of clouds with arbitrary geometry.

A test of our Monte Carlo model is presented in Fig. 1 (from Harshvardhan and Weinman, 1982b). The ratio of the reflection R of an array of cubic clouds to the reflection R' of an isolated cloud is calculated. All clouds have the same size and an optical depth of $\tau = 49$; the single scattering albedo is $\tilde{\omega} = 0.9999$ and a phase-function for a C.1 droplet size distribution is used. The solar zenith angle is $\theta = 0°$. The ratio R/R' is plotted versus $(s + d)/s$, where s is the cloud dimension and d the separation. As d approaches infinity, R/R' approaches 1, which is correct since clouds become isolated. For $d = 0$, the clouds merge to a single sheet. The interaction between clouds increases the local cloud albedo significantly for a separation of $d < 4s$. However, this local effect is drastically diminished if the average albedo of a cloud field is considered.

Our results in Fig. 1 include the interaction between a center cloud and its next neighbours, similar to Aida's (1977) approach. Harshvardhan and Weinman (1982b) used an approximate three-dimensional model, but they considered the radiative interaction between all cuboidal clouds which explains the differences.

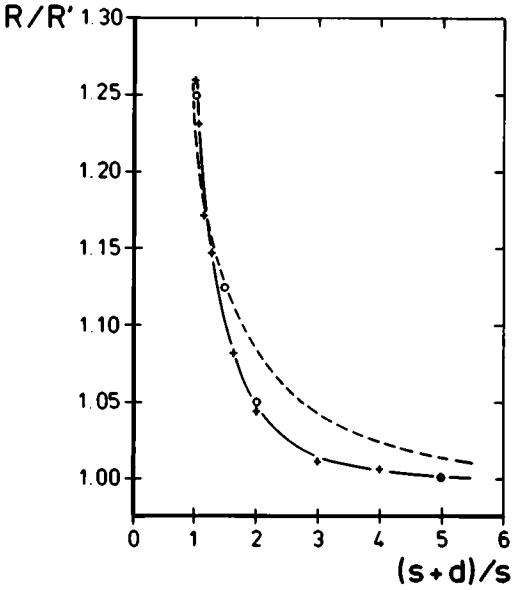

Fig. 1. Ratio of the reflection R from an array of cubic clouds to the reflection R' from an isolated cloud at a single wavelength ($\lambda = 450$ nm). O Aida (1977). --- Harshvardhan and Weinman (1982b). —— + this work. s is the cloud dimension and d the separation of individual cloud. Single-scattering albedo: $\tilde{\omega} = 0.9999$; optical depth: $\tau = 49$; zenith angle: $\theta_0 = 0°$.

In summary, Fig. 1 shows that our Monte Carlo scheme is in agreement with previous work (Aida, 1977), and it will be used in the following to derive a parameterization for the influence of cloud geometry or macrostructure on radiative properties.

7. Parameterization of cloud fields

It is an observable feature that the average cloud size of a cloud field increases as cloud amount increases (Plank, 1969). This can be simply explained by the merging of individual clouds. Plank observed such an increase for the horizontal as well as for the vertical extent of a cloud. Obviously this feature is not accounted for by a simple area weighting of radiative fluxes with actual cloud amount, nor is the concept of a regular array of identical cuboidal clouds compatible with that

observation. Fields of regular clouds are quite useful in studying the influence of radiative interactions between individual clouds (i.e., mutual shading and multiple reflection). While this interaction can significantly enhance the local cloud albedo, the mean cloud field albedo of the array is fairly well-described by a simple area weighting (Claussen, 1982). Claussen's result for a single visible wavelength is confirmed in Fig. 2, where the albedo of a field of identical interacting clouds is calculated from an integration over 8 solar wavelengths. The effective cloud cover N_e is calculated from the relation:

$$N_e = \frac{NR'}{R_\infty}, \tag{35}$$

where N is the actual amount (vertical projection of cloud on to the surface), R' is the albedo of a single cloud within the field, and R_∞ the albedo of an infinite cloud layer. Fig. 2 shows no systematic deviation of the effective cloud amount from the real cloud amount, except for $\theta = 0°$. Generally, deviations are of the order of 10%. It must be noted that the use of different cloud shapes results in slightly different results. The conclusion from Fig. 2 is that the cloud-cloud interaction plays a minor rôle for deviations from a linear relationship between cloud amount and mean optical properties of a cloud field.

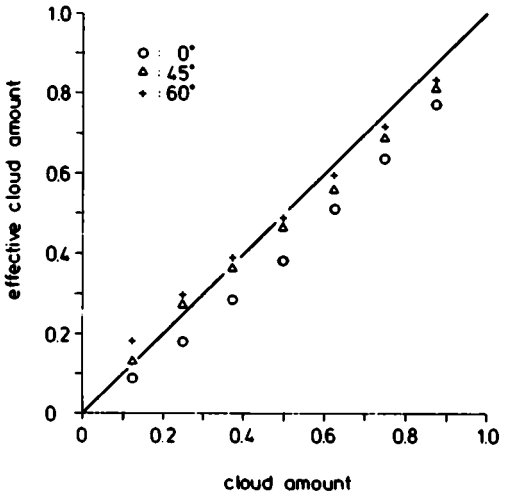

Fig. 2. Solar effective cloud cover (see eq. (35)) of a field of equally-sized cubic clouds versus actual cloud cover. The solid line is the one-to-one relation. The signs pertain to different solar zenith angles as denoted in the figure.

7.1. *Cloud size dependence on cloud amount*

In order to model the growth of the geometric cloud size with cloud amount, we adopted the following line of thought.

(1) Individual clouds consist of a cluster of unit elements.

(2) As cloud amount increases, the probability of clustering increases, and hence the average cloud size of the cloud size spectrum increases.

A simple mathematical model for cloud size as a function of cloud amount is assumed. Consider an infinite chain of unit elements where the probability that an element is cloudy is proportional to the cloud amount N (e.g., Stauffer, 1980). Then the probability for a clustering of q cloudy elements is N^q. The ends of the cluster have to be cloud-free, which gives twice the factor $(1 - N)$. The probability n for a cluster of size q is then:

$$n(q) = N^q(1 - N)^2. \tag{36}$$

The average cluster or cloud size $\bar{q}$ is then calculated as the ratio of two converging series:

$$\bar{q} = \frac{\sum_{q=1}^{\infty} n(q)\, q^2}{\sum_{q=1}^{\infty} n(q) q} = \frac{1 + N}{1 - N}, \tag{37}$$

where $q \in \mathrm{IN}$. A derivation of eq. (37) is given in the Appendix.

Eq. (37) provides the desired relation between average cloud size and cloud amount. It should be stressed that the units of $\bar{q}$ are not yet physical, but just the number of unit elements q. One has to define the optical dimensions (optical thickness) of such a unit element which will be done below. Eq. (37) will be extended to a two-dimensional cloud growth assuming that the growth is the same in both horizontal directions. In a further model, this growth will also be extended to the vertical direction. Fig. 3 illustrates how the average relative cloud size increases with cloud amount.

7.2. *Effective cloud cover*

In this subsection, three models for the parameterization of the radiative properties of broken cloud will be described.

7.2.1. *Model 1 (M1).* The simplest approach to model the radiative properties of a broken cloud layer is the commonly-used area weighting of the radiative characteristics (i.e. albedo, emittance, etc.) of a plane-parallel cloud with cloud amount. This approach is hereafter referred to as model 1 (M1).

7.2.2. *Model 2 (M2).* Monte Carlo calculations were performed for single finite clouds of varying size assuming that they represent the solar optical properties of a cloud field with a certain cloud amount. The cloud size is computed from cloud amount using eq. (37). Here the optical dimensions (i.e., the optical depths in the x, y, z directions) of a unit element are chosen as 10:10:10. The vertical optical depth is kept constant, but the horizontal optical dimensions vary according to eq. (37). For example, a cloud with the optical dimensions 12.9:12.9:10 is characteristic of 1 okta cloud amount, while the dimensions 150:150:10 are characteristic of 7 oktas. With increasing cloud amount, the height to width ratio (i.e. the aspect ratio) of the average cloud decreases and the average cloud approaches a single sheet as N goes to 1.

Monte Carlo simulations were performed for 3 zenith angles and for cloud amounts from 1 to 8 oktas. The effective cloud cover $N_{e,sol}$ was calculated from eq. (35), and the results were fitted with an empirical expression, relating $N_{e,sol}$ to the actual cloud amount:

$$N_{e,sol} = N^{(1.2+0.7N^2)}. \tag{38}$$

Eq. (38) yields the correct limits as N approaches 0 or 1. Fig. 4 shows that it is a reasonable fit to the Monte Carlo results for the three solar zenith angles. The results are integrations over 4 spectral intervals which were properly weighted with insolation. About 12,000 photons were traced in each spectral band.

The dotted line in Fig. 4 denotes Harshvardhan's (1982) parameterization of the solar effective cloud amount for a regular cloud field with the aspect ratio 1 (i.e., cloud cubes). It can be seen that N_e is larger than N which is in contrast to our paramaterization.

A comment on our assumption that the optical properties of a cloud field are represented by an average cloud should be added. Certainly there exists a single finite cloud whose optical properties are equal to the average properties of the cloud field, but it remains an assumption that this cloud is adequately described by eq. (37) and the empirical choice of the optical dimensions of a unit element.

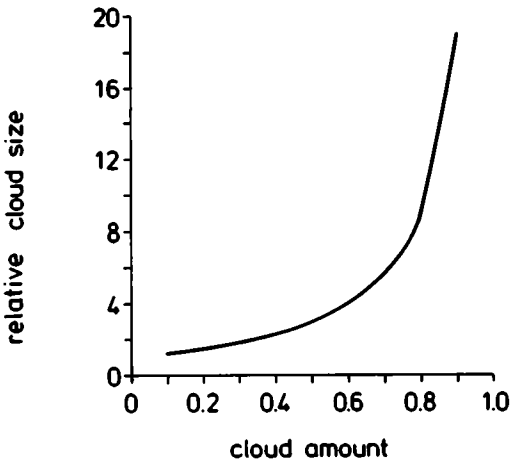

Fig. 3. Average relative cloud size as a function of cloud amount (after eq. (37)). The units of the cloud size are arbitrary and depend on the optical depth as a unit element (for details see text).

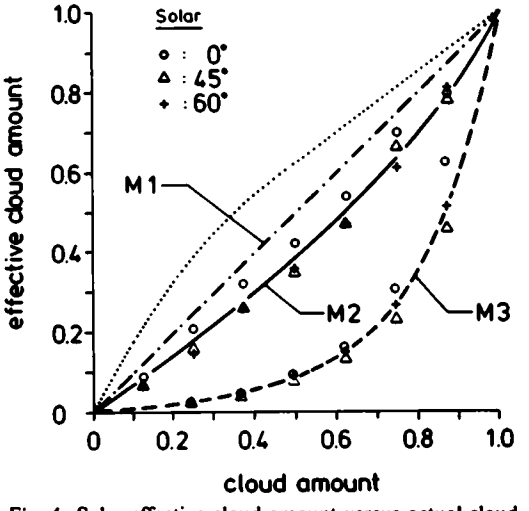

Fig. 4. Solar effective cloud amount versus actual cloud amount. Different signs denote wavelength-integrated Monte Carlo results for 3 zenith angles. Lines pertain to parameterizations for different cloud models. --- M1 (area weighting with cloud amount). —— M2 (cloud grows only in horizontal dimensions). M3 (cloud grows in three dimensions). ····· solar effective cloud amount after Harshvardhan (1982) (for details see text).

Experimental studies seem to be required to assess the validity of this choice. One example will be shown below in Subsection 7.2.4.

For the thermal infrared radiation, a formulation for the effective cloud amount $N_{e,IR}$ after Harshvardhan and Weinman (1982a) is adopted:

$$N_{e,IR} = \frac{\{1 + 2a(1 + 0.15)N\}N}{1 + 2aN(1 + 0.15N)}, \quad (39)$$

where a is the aspect ratio, defined as the ratio of height to width of the cubic cloud. Eq. (39) has been derived for an array of cubic clouds. The use of eq. (39) is made consistent with $N_{e,sol}$ derived from the Monte Carlo calculations by decreasing the aspect ratio "a" with increasing cloud amount according to eq. (37), i.e., here we have $a = 1/\bar{q}$. Although one could argue that the infrared and solar models are not fully consistent, such a consistency can be achieved by considering the solar parameterization as being valid for a field of non-interacting clouds whose aspect ratio varies according to eq. (37).

Fig. 5 shows the relation between $N_{e,IR}$ and N.

7.2.3. *Model 3 (M3).* Model 3 is a modification of model 2 also taking into account that the vertical optical depth of an average cloud increases as cloud amount increases. Again the optical dimensions of the cloud are varied according to eq. (37). Since all dimensions grow in the same way as cloud amount increases, the aspect ratio remains $a = 1$. In order to avoid vertical optical depths which are not realistic, a cloud amount of 7 oktas is chosen as the limit for a vertical cloud growth. At that cloud amount, the maximum vertical optical depth of 10 is reached. The Monte Carlo calculations are fitted with the relation:

$$N_{e,sol} = N^{(1.5+4N)}, \quad (40)$$

Eq. (39) is used in the thermal infrared with $a = 1$. However, the cloud emittance is a function of cloud cover due to the increase of the vertical optical depth with cloud amount (see Figs. 4 and 5).

It is of note that Monte Carlo calculations for optical depth between 10 and 30 essentially give the same relation for the solar effective cloud amount, which means eqs. (38) and (40) are valid for a range of realistic optical depths.

Furthermore, it must be stated that the extension of the one-dimensional clustering model to two dimensions can only be justified for cloud fields without a preferred spatial orientation. The assumption is certainly incorrect for cloud rolls where the average cloud is elongated rather than having the same dimension in all horizontal directions. The extension of the 1-d clustering to the vertical dimension (Model M3) is suggested by Plank's observation (1969) of cumulus clouds indicating an aspect ratio of 1.

7.2.4. *Testing the parameterization of broken clouds.* Fig. 6 shows a comparison of the parameterizations (Models 1, 2, 3) for solar radiation with measurements. The solar transmittance calculated with the full radiation scheme using the effective cloud parameterization is compared with aircraft measurements (Schmetz et al., 1983) of the solar transmittance of a broken stratocumulus layer. The vertical optical depth of the plane-parallel cloud is chosen as $\tau = 10$ in order to fit the observations with overcast sky. Fig. 6 clearly shows that M1 does not describe the observations properly while M2 and, in this case, especially M3 are more adequate. As Fig. 2 has shown a regular array of cubic clouds, neither would describe the observations. Thus one is led to the conclusion that the radiative properties of cloud fields are mainly determined by cloud amount and the optical dimensions of the individual clouds, which is accounted for in models M2 and M3.

Whether models M2 and M3 are quantitatively valid certainly requires further measurements. It is

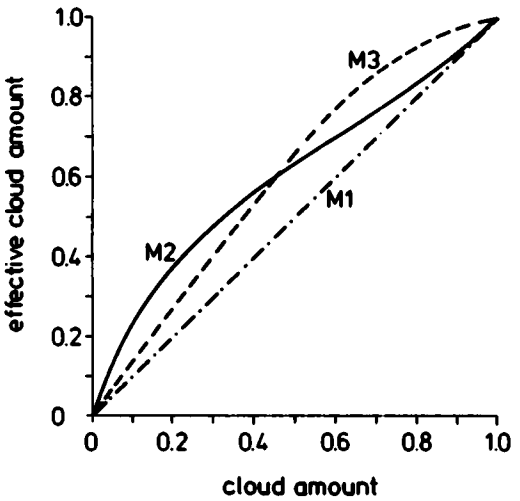

Fig. 5. Infrared effective cloud amount versus actual cloud amount. Different curves pertain to different cloud models as in Fig. 4.

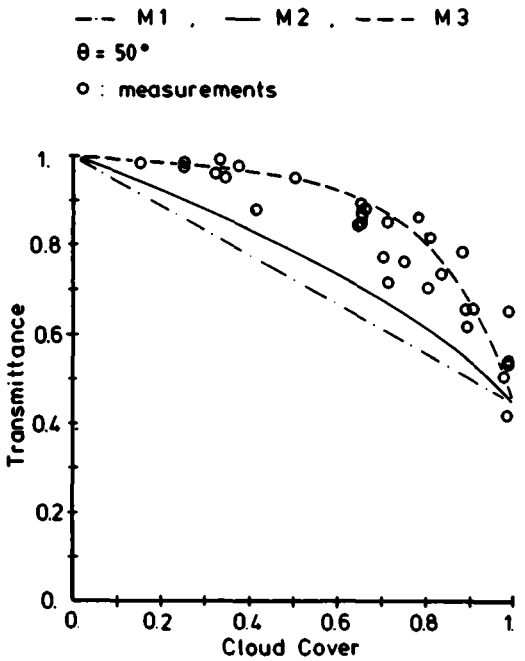

Fig. 6. Solar transmittance of a broken stratocumulus deck, as measured with an aircraft, versus cloud amount, and the transmittance curves computed from cloud models M1, M2 and M3. The solar zenith angle is 50° and the optical depth of the extended cloud layer is τ (0.55 μm) = 10.

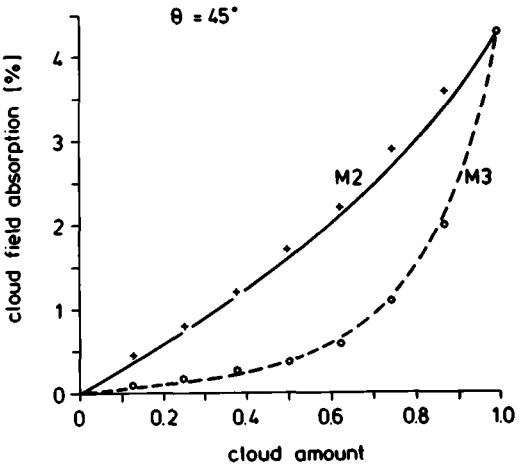

Fig. 7. Cloud field absorption versus cloud amount. Comparison between exact Monte Carlo results and the parameterization using the effective cloud cover for solar reflection. Solar zenith angle is $\theta = 45°$. M2 and M3 are different cloud models.

quite possible that the simple mathematical model for cloud growth as described in Subsection 7.1 is an oversimplification.

As an internal test of the solar parameterization, Fig. 7 shows the cloud field absorption as a function of cloud amount for M2 and M3 and a zenith angle of $\theta = 45°$, The absorption A is calculated from:

$$A(N) = A_\infty N_{\epsilon,\mathrm{sol}}. \tag{41}$$

This functional relationship is compared with the exact Monte Carlo results and shows good agreement. Thus, the effective cloud amount for the albedo is in good agreement with the effective cloud amount for absorption.

8. Application of the scheme

8.1. *Sensitivity parameters for broken clouds*

In Section 2, the cloud sensitivity parameters $\partial\alpha/\partial N$, $\partial F/\partial N$, and δ have been described. In this section, we apply the radiative transfer scheme (Sections 3 and 4) using the effective cloud cover parameterizations (Section 7) to estimate the effect of the brokenness of cloud on the sensitivity parameters. A model atmosphere characteristic of a mid-latitude summer including a maritime standard aerosol profile is assumed; surface albedo is 0.1, cloud top at 2 km and the vertical liquid water path of the infinite cloud layer is 0.05 kg m^{-2}, corresponding to an optical depth of τ (0.55 μm) = 13.1. Model runs are performed for cloud amount from 0 to 1 with increments of 0.1. The partial derivatives $\partial\alpha/\partial N$ and $\partial F/\partial N$ are then approximated by finite differences.

Fig. 8 shows the dependence of $\partial\alpha/\partial N$ on cloud amount. Results are given for two solar zenith angles and the three different effective cloud cover parameterizations M1, M2 and M3. The planetary albedo for clear sky is $\alpha = 0.114$ for $\theta = 0°$ and $\alpha = 0.164$ for $\theta = 60°$, while the corresponding values for $N = 1$ are $\alpha = 0.425$ and $\alpha = 0.52$, respectively. For model M1, where no 3-d effects are considered, $\partial\alpha/\partial N$ only increases slightly with cloud amount. This increase by about 10% is explained by the decreasing trapping of photons underneath the cloud layer as cloud amount increases. The differences in $\partial\alpha/\partial N$ for the two zenith angles are of the order of 10%.

For model M2, $\partial\alpha/\partial N$ is a distinctly increasing function of N. At cloud amounts smaller than

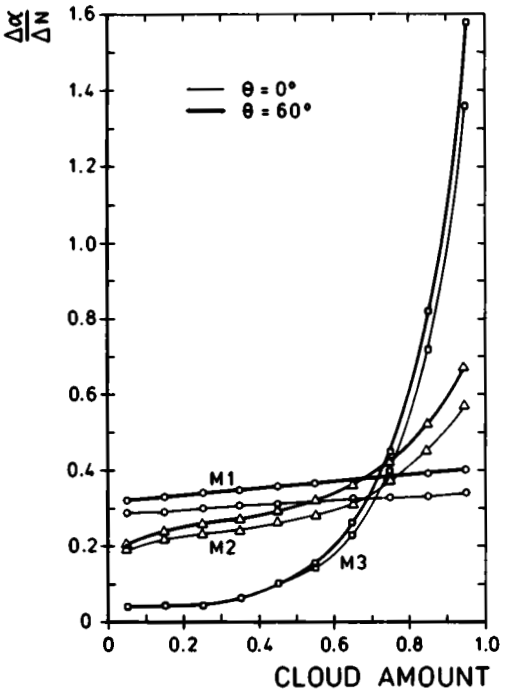

Fig. 8. Change of the planetary albedo α with cloud amount N versus cloud amount for 3 cloud models M1 (circles), M2 (triangles) and M3 (squares) and 2 solar zenith angles. The optical depth of the infinitely-extended cloud is $\tau(0.55\ \mu m) = 13.1$, cloud top is 2 km, surface albedo is 0.1, and a mid-latitude summer atmosphere with a maritime aerosol profile is used. $\theta = 0°$ corresponds to the thin line, $\theta = 60°$ to the heavy line.

about 0.7, the values are lower than the corresponding values of $\partial\alpha/\partial N$ for M1, while for large N the reverse is observed. The reason for this is the larger transmittance of finite clouds due to the leaking of photons through the cloud sides. This is accounted for in model M2, while M1 is merely a weighting of the planiform cloud with cloud amount. As cloud amount gets larger, individual clouds merge which is modelled by increasing the average cloud size. Then the cloud field albedo approaches the planiform albedo and $\partial\alpha/\partial N$ is larger than the corresponding values for M1.

While in model M2 the vertical optical depth of the finite cloud representing the cloud field is kept constant, it increases with cloud amount in model M3. Therefore the non-linear dependence of $\partial\alpha/\partial N$ on N is more extreme than for M2. The cross-over point where $\partial\alpha/\partial N$ exceeds the corresponding value for M1 is again at about $N = 0.7$.

The main conclusion from Fig. 8 is that the albedo effect of broken cloud is always lower than that of a plane-parallel cloud for cloud amounts lower than about $N = 0.7$. The reverse is correct for N larger than 0.7. This statement is not in accordance with the results of Harshvardhan (1982) who did different experiments with a regular array of cuboidal clouds. In his three experiments, Harshvardhan (1982) found an increased albedo effect for broken cloud at low cloud amounts (~0.2–0.3) and in one of his experiments a systematically increased albedo effect for all cloud amounts.

Fig. 9 shows the sensitivity of the outgoing long-wave flux to changes in cloud amount versus cloud for the three parameterizations of the effective cloud amount. M1 does give a constant $\partial F/\partial N = 13.6$ W m^{-2} since the effective cloud amount is equal to the cloud amount. For model M2, the greenhouse effect is enhanced if N is lower than about 0.2–0.3, i.e., the outgoing long-wave flux is more strongly reduced than in the case of a planiform cloud weighted with cloud amount. The greenhouse term $-\partial F/\partial N$ has a minimum for M2 at $N \approx 0.65$ which is explained by the fact that the aspect ratio of the average cloud approaches zero as N goes to 1. For M3, we find a steadily decreasing value for the greenhouse effect with a crossover point between M1 and M3 at about $N = 0.6$.

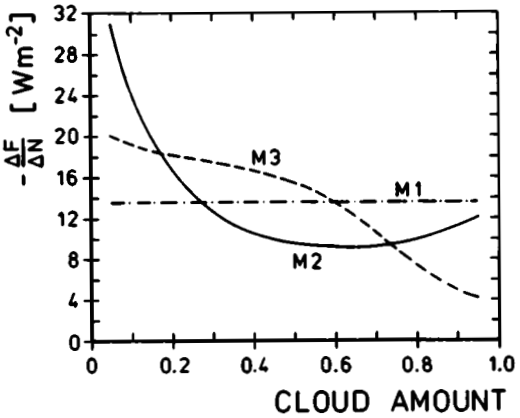

Fig. 9. Change of the outgoing long-wave flux F with cloud amount versus cloud amount for 3 cloud models M1, M2 and M3 (note that $\partial F/\partial N$ is negative). Cloud and atmosphere are as in Fig. 8.

The conclusion from Fig. 9 is that broken clouds do have a larger greenhouse effect than planiform clouds for small cloud amounts and vice versa for large cloud amounts. This is in qualitative agreement with Harshvardhan's (1982) results (his experiments two and three), which was to be expected since we used the same parameterization for the effective cloud amount in a modified way.

Fig. 10 provides an estimate of the dependence of the net radiative effect δ on cloud amount. The sign of this quantity determines whether the earth-atmosphere system gains (positive) or loses (negative) radiative energy if cloud amount increases. In Fig. 10, the values of δ are negative, indicating that the albedo effect dominates, which is a well-known effect of low cloud. The figure is essentially an image of Fig. 8, indicating the dominant character of the albedo. Models M2 and M3 show a strong non-linear increase of $-\delta$ with cloud amount; there exists a crossover point between M1 and M2 or M3. The essence is that similar changes in the amount of broken cloud lead to different net radiative effects depending on the actual value of cloud amount. Specifically, for small cloud amounts, broken clouds do have a larger net effect than planiform cloud and vice versa for large cloud amount.

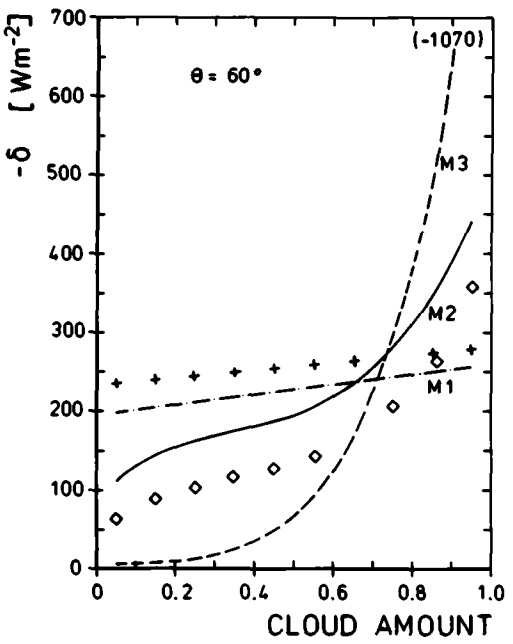

Fig. 10. Net radiative effect δ (see eq. (1)) as a function of cloud amount (note that δ is negative) for 3 cloud models (M1: dash-dotted; M2: solid; M3: dashed line). Cloud and atmosphere are as in Fig. 8 and the solar zenith angle is $\theta = 60°$. Crosses (+) denote results of a run using the M1 cloud but neglecting atmospheric aerosol. Diamonds (◇) show results for an M2 run, increasing the surface albedo from 0.1 to 0.3.

The finding should have use in the derivation of the net radiative effect of cloud from satellite measurements (e.g., Ohring and Clapp, 1980). Appropriate values for $\partial\alpha/\partial N$, dependent on N could be derived from high-resolution satellite images or aircraft measurements. Such experimental studies would also be useful in order to assess the validity of the effective cloud cover parameterization used in the present study.

8.2 *Sensitivity parameters and atmospheric conditions*

The magnitude of the sensitivity parameter δ also depends on surface and atmospheric properties. An example of this is also shown in Fig. 10 (marked with +). The radiation scheme has been run for the same atmospheric conditions as above using the M1 model, except that the atmosphere is taken as aerosol-free. The neglect of aerosol scattering and absorption results in a decrease of δ from -200 W m^{-2} to -232 W m^{-2}. This is due to the increased albedo effect, since the neglect of aerosols lowers the planetary albedo of the clear atmosphere from 0.164 to 0.132, which in turn enhances the difference between clear and cloudy planetary albedo.

The diamonds (◇) in Fig. 10 denote results of a run using model M2, with a surface albedo increased from 0.1 to 0.3. The contrast between cloud-free and cloudy planetary albedo is decreased, which decreases the albedo effect of clouds and increases δ on the average in this case by more than 100 W m^{-2}.

The last two experiments demonstrate that studies of the net radiative effect of clouds are significantly dependent on the atmospheric and surface conditions. Therefore it is useful to conduct studies with radiation schemes taking account of realistic atmospheric conditions.

8.3. *Bispectral curves for broken clouds*

With the aid of the detailed radiation scheme, it is possible to construct bispectral curves (visible

and IR). These curves are used to discriminate between dominating scenes in a satellite image, where the different scenes appear as clusters of pixels (e.g., Desbois et al., 1982).

Recently, Platt (1983) suggested that the existence of distinctive bispectral curves for cloud signature could be used to deduct detailed cloud information from visible and IR channels of satellites. In particular, he stated that extended cloud layers with varying optical depth follow a curve in a histogram of visible versus IR pixels, while broken layers show a straight line.

This is examined in Fig. 11. The planetary albedo of a cloud field is plotted as a function of the effective black-body temperature of the outgoing long-wave flux. The model assumptions are the same as in Subsection 8.1. The lines in Fig. 11 give the transition from cloud-free to overcast sky for the 3 cloud models described in Subsection 7.2, and the signs mark the results for a cloud amount from $N = 0$ to 1 with 0.1 increments. Cloud Model M1 agrees with Platt's approach in handling broken cloud and approximately shows the expected straight line. However, for M2 and M3, a well defined "J"-shape of the bispectral curve is to be observed, although the curves are quantitatively different. Thus, the inclusion of the three-dimensional characteristics of clouds leads to a signature which is qualitatively similar to that of an infinite cloud layer with varying optical depth. This is verified by the inclusion of model results for an unbroken cloud in Fig. 11. The crosses correspond to calculations where the area-averaged liquid water is the same as that for the cloud models M1 and M2. Here, the "J"-shape is less extreme than for model M3 but more pronounced than for model M2.

One can conclude that the "J" shape signature is typical for realistic broken and unbroken cloud layers with horizontal and vertical variability. This qualitative agreement of the signatures of extended and broken clouds seems to prevent a possible discrimination between these cloud structure types from two-dimensional histograms. But the extraction of higher moments of the area-averaged IR and visible measurements might bear useful information. Broken cloud should exhibit large standard deviations in the IR and VIS channels. Unbroken cloud is expected to show significantly less variability in the IR since clouds reach an

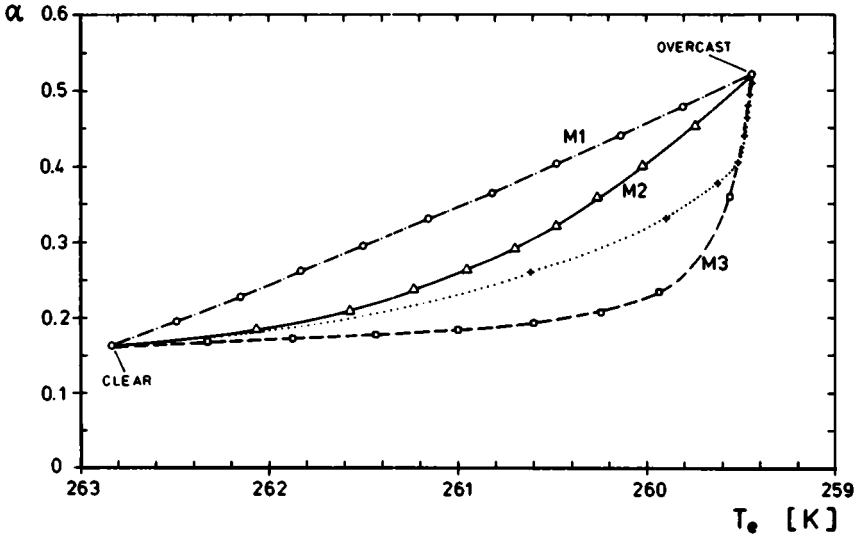

Fig. 11. Bispectral curves calculated with the radiation scheme for cloud models M1 (dash-dotted), M2 (solid) and M3 (dashed). The planetary albedo versus the effective black-body temperature of the outgoing long-wave flux is plotted. The lines give the transition from clear to overcast sky. Signs indicate the results for cloud amounts from 0 to 1 with 0.1 increments. Crosses (dotted line) pertain to a planiform cloud whose liquid water path (optical depth) is steadily increased so that the area-averaged liquid water is equal to that in models M1 and M2.

emittance of 1 for a liquid water path (LWP) of only ~40 gm^{-2}. The VIS (albedo) signal is not yet saturated at this LWP value. Thus unbroken cloud with horizontal variable optical depth should show relatively high VIS and low IR standard deviations. Coakley and Bretherton (1982) have used such a method in the IR to deduce cloud signature parameters from satellite observations.

9. Summary and conclusions

In this study, a radiative transfer scheme has been developed which includes explicitly fractional cloud amount. The scheme accounts for gaseous and aerosol absorption and scattering. The optical properties of the cloud are consistently determined for the solar and thermal radiation from spectral values of the microphysical parameters of the cloud droplet size distributions (single scattering albedo, extinction coefficient and asymmetry parameter). The scheme allows for detailed studies of the radiative effects of fractional cloud amounts interacting with realistic atmospheric and surface conditions.

The effects of broken cloud are parameterized as an effective cloud amount which is used for weighting the radiative properties of planiform clouds. The parameterizations are derived from wavelength-integrated Monte Carlo simulations for the solar radiative properties of cloud fields. In the thermal region, a formulation after Harshvardhan and Weinman (1982a) is adopted. We do not follow the previously used concept of a regular array of identical clouds. The basic assumption for the cloud fields is that the average cloud size increases with cloud amount and that the mean radiative properties of cloud fields are represented by the average cloud. The cloud growth with cloud amount is derived from a simple statistical model.

In contrast with previous studies (Harshvardhan, 1982), it is found that the solar effective cloud cover of a broken cloud layer—as defined by eq. (35)—is always less than the actual cloud cover with the same vertical depth, while the opposite is true for infrared radiation if the emittance is 1, i.e., the radiative characteristic of a field of clouds retains the single cloud characteristic which is determined by the leaking of photons through the cloud sides.

A comparison of the solar radiative transfer scheme with measured data from an aircraft flight under a broken stratocumulus deck shows qualitative agreement, which increases confidence in the idealized model for the cloud growth with cloud amount. This growth in turn implies a non-linear relation between mean radiative properties of cloud fields and cloud amount. This is also in agreement with other observations relating cloud radiative properties to actual cloud amount (e.g., Kasten and Czeplak, 1980; Hughes and Henderson-Sellers, 1983). A regular array of identical clouds does not reproduce the observations, even though cloud-cloud interaction, i.e., mutual shading and multiple reflection, is simulated.

Since large fractions of the globe are covered with broken cloud, it is important to study the net radiative effect of a variation in broken cloud. Therefore, the radiation scheme is applied to calculate this net effect. Due to the non-linearity between mean solar or IR radiative properties and cloud amount, the net radiative effect is strongly dependent on cloud amount. Thus, similar changes ΔN in cloud amount N can lead to completely different net effects, depending on the absolute amount of cloud.

It is found that for cloud amounts less than 0.7, the albedo effect of a broken layer is lower than that of a planiform cloud, while the relation is reversed for larger cloud amounts. The greenhouse effect of broken cloud is higher than the corresponding effect of planiform cloud at low cloud amounts, while the opposite is observed for large cloud amounts. Thus both effects are changed in the same direction and do not cancel. That is to say, in case of small cloud amount and a broken cloud layer, the earth-atmosphere system gains more or loses less radiation energy than for a planiform cloud. At high cloud amount, broken clouds exhibit a stronger albedo effect and a smaller greenhouse effect than planiform cloud.

The application of a constant value of $\partial\alpha/\partial N$ and $\partial F/\partial N$ for the determination of the net effect δ (see eq. 1) seems to be incorrect. The use of a constant value is only valid for extended horizontally homogeneous clouds where the radiation field for partial cloud cover can be described by simple area weighting with cloud amount. In order to get a better estimate of the global net effect, a cloud climatology is required which includes cloud amount and some measure of the brokenness of cloud (for instance variances).

Furthermore, the radiation scheme is applied to compute the bispectral curve of a broken cloud layer. A "J" shape is a typical feature if the IR is plotted against the visible. This is true for broken cloud layers as well as for extended layers with horizontally variable optical depth. The qualitative agreement does not allow us to distinguish between broken and unbroken clouds just from the shape of the bispectral curve.

It must be stressed that the results for the effects of broken cloud are certainly dependent on the cloud model. In this study, a purely statistical relation is used to determine the average cloud size of a cloud field and thereby its radiative properties. Therefore, the study performed in Section 7 can only partially answer the question of the net radiative effect of broken cloud. Further, studies have to show if the concept of using an average cloud to describe the radiative properties of cloud fields is reasonable or an oversimplification. However, it should also be said that is was the intention of the exercise to simplify and idealize. The use of effective cloud amounts to describe cloud fields seems to be very useful since it enables us to simulate the mean radiative properties of such fields with one-dimensional models.

Since the radiation scheme has a high spectral resolution, further studies are possible, simulating the exact response characteristics of satellite sensors and relating these spectral quantities to integrated ones. Preliminary results show that generally, this spectral correction is essential. The scheme is also appropriate for using existing cloud climatologies as model input to estimate the global net radiative effect of cloud.

10. Acknowledgements

I thank Professors H. Graßl and H. Hinzpeter, Dr. M. Beniston, and Mrs. M. Newiger for reading the manuscript and for helpful comments. Thanks are due to Mrs. B. Zinecker for typing the manuscript.

11. Appendix

Derivation of the average cluster size

For $|N| < 1$ and $q \in \mathbb{N}$, the infinite geometrical series N^q converges:

$$\sum_{q=0}^{\infty} N^q = \frac{1}{1-N} \tag{A1}$$

By repeated differentiation, one finds for any natural number p:

$$\sum_{q=0}^{\infty} \binom{q+p}{q} N^q = \frac{1}{(1-N)^{p+1}}, \tag{A2}$$

where $\binom{q+p}{q}$ are the binomial coefficients.

For the first moment of the function $n(q) = N^q(1-N)^2$ (see eq. (36)), we find

$$\sum_{q=1}^{\infty} qN^q(1-N)^2 = (1-N)^2 \times \left\{ \sum_{q=0}^{\infty} (q+1)N^q - \sum_{q=0}^{\infty} N^q \right\} = N. \tag{A3}$$

Using eq. (A2) with $p = 2$ we have:

$$\frac{1}{(1-N)^3} = \frac{1}{2}\left\{ \sum_{q=0}^{\infty} q^2 N^q + \sum_{q=0}^{\infty} 3qN^q + \sum_{q=0}^{\infty} 2N^q \right\}. \tag{A4}$$

With the aid of eq. (A4), the second moment of $n(q)$ can easily be calculated:

$$\sum_{q=1}^{\infty} q^2 N^q (1-N)^2 = \frac{N+N^2}{1-N}. \tag{A5}$$

The ratio of eq. (A5) to (A3) yields eq. (37).

REFERENCES

Aida, M. 1977. Scattering of solar radiation as a function of cloud dimensions and orientation. *J. Quant. Spectrosc. Radiat. Transfer 17*, 303–310.

Busygin, V. P., Yestratov, N. and Feigelson, E. 1973. Optical properties of cumulus and radiation fluxes of cumulus cloud cover. *Izv. Atmos. Ocean Phys. 9*, 1142–1151.

Cess, R. D. 1976. Climate changes: an appraisal of

atmospheric feedback mechanisms employing zonal climatology. *J. Atmos. Sci. 33*, 1831–1843.

Claussen, M. 1982. On the radiative interaction in three-dimensional cloud fields. *Contrib. Atmos. Phys. 5*, 158–169.

Coakley, J. A. and Bretherton, F. P. 1982. Cloud cover from high-resolution scanner data: detecting and allowing for partially filled fields of view. *J. Geophys. Res. 87*, 4917–4932.

Davies, R. 1978. The effect of finite cloud geometry on the three-dimensional transfer of solar radiation through clouds. *J. Atmos. Sci. 35*, 1712–1725.

Deirmendjian, D. 1969. *Electromagnetic scattering on polydispersions*. American Elsevier Publishing Comp., New York.

Desbois, M., Seze, G. and Szejwach, G. 1982. Automatic classification of clouds on Meteosat imagery: application to high-level clouds. *J. Appl. Meteorol. 21*, 401–412.

Fouquart, Y. and Morcrette, J. 1981. Sensitivity of the radiation field to cloud cover. Workshop on radiation and cloud-radiation interaction in numerical modelling, ECMWF.

Geleyn, J. F., Hense, A. and Preuß, H. J. 1982. A comparison of model-generated radiation fields with satellite measurements. *Contr. Atmos. Phys. 55*, 253–286.

Gube, M., Schmetz, J. and Raschke, E. 1981. Solar radiative transfer in a cloud field. *Contrib. Atmos. Phys. 53*, 24–34.

Harshvardhan, 1982. The effect of brokenness on cloud-climate sensitivity. *J. Atmos. Sci. 39*, 1853–1861.

Harshvardhan and Weinman, J. 1982a. Infrared radiative transfer through a regular array of cuboidal clouds. *J. Atmos. Sci. 39*, 431–439.

Harshvardhan and Weinman, J. 1982b. Solar reflection from a regular array of horizontally-infinite clouds. *Appl. Optics 21*, 2940–2944.

Hartmann, D. A. and Short, D. A. 1980. On the use of earth radiation budget statistics for studies of clouds and climate. *J. Atmos. Sci. 37*, 1233–1250.

Herman, G. F., Wu, M. and Johnson, W. T. 1980. The effect of clouds on the earth's solar and infrared radiation budgets. *J. Atmos. Sci. 37*, 1251–1261.

Hughes, N. and Henderson-Sellers, A. 1983. A preliminary global oceanic cloud climatology from satellite albedo observations. *J. Geophys. Res. 88*, 1475–1483.

Hunt, G. E. 1982. On the sensitivity of a general circulation model climatology to changes in cloud structure and radiative properties. *Tellus 34*, 29–38.

Kasten, F. and Czeplak, G. 1980. Solar and terrestrial radiation dependent on the amount and type of cloud. *Solar Energy 24*, 177–189.

Marchuk, G. J., Mikhailov, G. A., Nazaraliev, M. A., Dorbinjan, R. A., Kargin, B. A. and Elepov, B. S. 1980. *The Monte Carlo methods in atmospheric optics*. Springer-Verlag, Berlin–Heidelberg–New York.

McClatchey, R. A., Bolle, H.-J. and Kondratyev, K. Ya. 1980. A cloudless standard atmosphere for radiation computations. Report of the Radiation Commission of the IAMAP. Available through the Radiation Commission.

McKee, T. B. and Cox, S. K. 1974. Scattering of visible radiation by finite clouds. *J. Atmos. Sci. 31*, 1885–1892.

Ohring, G. and Clapp, P. 1980. The effect of changes in cloud amount on the net radiation at the top of the atmosphere. *J. Atmos. Sci. 37*, 447–454.

Plank, V. 1969. The size distribution of cumulus in representative Florida populations. *J. Appl. Meteorol. 8*, 46–57.

Platt, C. M. R. 1983. On the bispectral method for cloud parameter determination from satellite VISSR data: Separating broken cloud and semitransparent cloud. *J. Appl. Meteorol. 22*, 429–439.

Potter, J. F. 1970. The delta-function approximation in radiative transfer theory. *J. Atmos. Sci. 27*, 943–949.

Schmetz, J. and Raschke, E. 1979. An application of a two-stream approximation to calculations of the transfer of solar radiation in an atmosphere with fractional cloud cover. *Contrib. Atmos. Phys. 52*, 151–160.

Schmetz, J., Raschke, E. and Fimpel, H. 1981. Solar and thermal radiation in maritime stratocumulus clouds. *Contrib. Atmos. Phys. 54*, 442–452.

Schmetz, J., Slingo, A., Nicholls, S. and Raschke, E. 1983. Case studies of radiation in the cloud capped atmospheric boundary layer. *Phil. Trans. R. Soc. Lond. A. 308*, 377–388.

Schneider, S. H. 1972. Cloudiness as a global climatic feedback mechanism: the effects on the radiation balance and surface temperature variations in cloudiness. *J. Atmos. Sci. 29*, 1413–1422.

Slingo, A., Nicholls, S. and Schmetz, J. 1982. Aircraft observations of marine stratocumulus during JASIN. *Q. J. R. Meteorol. Soc. 108*, 833–856.

Stauffer, D. 1980. Perkolation—der einfachste Phasenübergang? *Phys. Bl. 36*, 124–126.

Wang, W. C., Rossow, W. B., Yao, M. S. and Wolfson, M. 1981. Climate sensitivity of a one-dimensional radiative-convective model with cloud feedback. *J. Atmos. Sci. 38*, 1167–1178.

Welch, R. M. and Zdunkowski, W. G. 1981. The radiative characteristics of non-interacting cumulus cloud fields (I). Parameterization of finite clouds. *Contrib. Atmos. Phys. 54*, 258–272.

Wetherald, R. T. and Manabe, S. 1980. Cloud cover and climate sensitivity. *J. Atmos. Sci. 37*, 1485–1510.

Zdunkowski, W. G., Welch, R. M. and Korb, G. 1980. An investigation of the structure of typical two-stream-methods for the calculation of solar fluxes and heating rates in clouds. *Contrib. Atmos. Phys. 53*, 147–166.